

Dust–Gas Accretion onto a Luminous Object

Jun FUKUE

*Astronomical Institute, Osaka Kyoiku University, Asahigaoka, Kashiwara, Osaka 582-8582
fukue@cc.osaka-kyoiku.ac.jp*

(Received 2000 December 11; accepted 2001 January 25)

Abstract

Spherical accretion of dust and gas onto a gravitating object is examined under the influence of central radiation. We found that, as long as the central luminosity is less than the Eddington one for dust, the gas flow is almost Bondi type, while the dust flow is greatly affected by central radiation. For non-luminous sources, in the outer region where the gravity on the dust is balanced by the drag force, the infall velocity of dust is generally larger than the gas velocity. Both gas and dust freefall in the inner region. As the dust-to-gas ratio increases, the gas accretion rate slightly decreases, while the dust accretion rate increases. As a result, the total accretion rate increases. When the central luminosity is considered, the infall velocity of dust becomes smaller and smaller, as the central luminosity increases. Although the gas accretion rate slightly increases with luminosity, the dust accretion rate linearly decreases due to the radiation pressure. As a result, the total accretion rate decreases with luminosity. Approximate expressions for dust and gas accretion rates were obtained.

Key words: accretion — black hole physics — dust — radiation — stars: formation

1. Introduction

Mass accretion onto a central gravitating object is one of the key processes of astrophysics, since the accretion process releases enormous gravitational energy. Since Bondi (1952) and Henriksen and Heaton (1975), as well as accretion disks (Shakura, Sunyaev 1973), spherical and disk accretion has been extensively investigated by many authors (see, e.g., Kato et al. 1998 for a review).

Relating to accretion, the effect of radiation of a central object, whether the central star originally shines or the accreting gas radiates, has been also examined; for spherical accretion (e.g., Shapiro 1973; Tamazawa et al. 1975; Burger, Katz 1980; Flammang 1982), with radiation drag (Umemura, Fukue 1994), for Hoyle–Lyttleton case (Taam et al. 1991; Nio et al. 1998), for disk case (Fukue, Umemura 1995). In these studies, a fully ionized plasma was generally assumed and the electron scattering interaction was usually considered, since accretion onto a black hole was often supposed.

As is well known, dust grains, such as graphites and silicates, are strongly influenced by radiation, since the cross-section per mass is large (typically, the dust opacity is thousand times larger than the electron scattering one). In the current study of the accretion process, however, it seems that the effect of radiation in the dust–gas flow has been scarcely examined.

On the other hand, dust-driven winds from red giants and AGB stars have been extensively studied. For example, the momentum coupling between dust grains and the gas was firstly proposed by Gilman (1972). Since then, dust-driven winds have been studied by many researchers (Goldreich, Scoville 1976; Berruyer, Frisch 1983; Tielens 1983; Gail, Sedlmayr 1987; MacGregor, Stencel 1992; Netzer, Elitzur 1993; Krüger et al. 1994). In these dust-driven winds dust grains are pushed outwards by stellar radiation, and then the gas is dragged by the frictional force to gain additional momentum. The gas tem-

perature is raised considerably above its radiative equilibrium value due to frictional heating between dust and gas (Krüger et al. 1994).

There may be several reasons for the fact that little attention has been paid to the radiative effect on dust–gas accretion. One is that the attention of researchers was mainly focused on the high-energy regime, such as a black-hole accretion, where the gas is fully ionized and dust is absent. Another is that in such a field of the star-forming region, attention was focused on the energy-transfer problem between dust and radiation, rather than the momentum coupling in the dynamical flow.

In recent years the importance of dust grains has become recognized. Besides protoplanetary disks, even in the case of black-hole accretion, black holes may be embedded in molecular clouds. There exist many (young) AGNs and Seyferts with dusty envelopes. Taking a broad view of dust–gas flow under radiation fields in such active objects as protoplanetary disks, proto-planetary nebula formation, black-hole accretion, accretion disk winds, jets, and young AGNs, we shall fill up the lack of research in this field: we first examine the spherical accretion of dust and gas under central radiation.

In the next section the basic equations are described. Transonic solutions are obtained and applied to astrophysical objects in section 3. The present results are discussed in section 4. The final section is devoted to concluding remarks.

2. Basic Equations

Let us suppose stationary, spherically-symmetric accretion of dust and gas onto a central gravitating body of mass M . The flow is assumed to be optically thin (at least for dust), and affected by the radiation field of the central object, if it shines. The magnetic field and self-gravity of the gas are neglected.

The basic equations for such a dust–gas flow are found in the literatures of dust-driven winds (see, e.g., Krüger et al. 1994;

Lamers, Cassinelli 1999). Based upon Lamers and Cassinelli (1999), the basic equations for the present case are described as follows.

2.1. Dust Opacity

In general, the size of dust grains distributes over some ranges, and grains with different size move with different velocities. We assume, for simplicity, that the dust grains have a uniform size a_d (a typical size is $a_d = 0.05 \mu\text{m}$). Hence, the geometrical cross-section σ_d and mass m_d of a dust grain are also uniform: $\sigma_d = \pi a_d^2$ and $m_d = (4/3)\pi a_d^3 \hat{\rho}$, where $\hat{\rho}$ is the grain density (typically, $\hat{\rho} \sim 2.2 \text{ g cm}^{-3}$ to 3.3 g cm^{-3} for graphites to silicates; see, e.g., Gilman 1972).

The dust opacity κ_d is approximately expressed as

$$\begin{aligned} \kappa_d &= \frac{\sigma_d}{m_d} Q_A \\ &= 0.68 \times 10^3 \text{ cm}^2 \text{ g}^{-1} \\ &\quad \times \left(\frac{\hat{\rho}}{2.2 \text{ g cm}^{-3}} \right)^{-1} \left(\frac{a_d}{0.05 \mu\text{m}} \right)^{-1} \left(\frac{Q_A}{0.01} \right), \end{aligned} \quad (1)$$

where Q_A is the absorption efficiency, which is of the order of 10^{-2} in the temperature range of 10^2 to a few $\times 10^3 \text{ K}$ (Lamers, Cassinelli 1999). We assume that the dust opacity is constant throughout this paper.

In addition, we ignore the dust formation or destruction in the relevant range. Before accretion takes place, the dust grains are assumed to form in the environment of a surrounding gas cloud. In the vicinity of the central object, the dust grains would evaporate and be destroyed, since the temperature becomes high and the central radiation is so intense. However, the mass accretion rate does not depend on such a state of the central region, where supersonic flow is attained. It is determined by the transonic condition as an eigenvalue. Hence, as long as the temperature at the sonic point is sufficiently low, we can safely ignore the dust evaporation to determine the accretion rate.

2.2. Continuity Equations

Since we ignore the dust formation and destruction, the mass conservations for the gas and dust components are, respectively,

$$4\pi r^2 \rho v = -\dot{M}, \quad (2)$$

$$4\pi r^2 \nu u = -\dot{M}_d, \quad (3)$$

where ρ is the gas density, v the gas infall velocity, \dot{M} the gas accretion rate, ν the dust density, u the dust infall velocity, and \dot{M}_d the dust accretion rate.

2.3. Equations of Motion

When the central object or the accreting gas radiates at luminosity L , the dust grains suffer from radiation pressure, while the gas component does not. The equations of motion in the radial direction for the present case are generally written as

$$v \frac{dv}{dr} = -\frac{1}{\rho} \frac{dp}{dr} - \frac{GM}{r^2} + \frac{1}{\rho} f_{\text{drag}}, \quad (4)$$

$$u \frac{du}{dr} = -\frac{GM(1-\Gamma)}{r^2} - \frac{1}{\nu} f_{\text{drag}}, \quad (5)$$

where p is the gas pressure, f_{drag} the collisional drag force exerted on the gas due to drifting dust grains, and Γ the normalized luminosity, defined as

$$\Gamma = \frac{\kappa_d L}{4\pi c G M}. \quad (6)$$

It should be noted that $4\pi c G M / \kappa_d$ is the Eddington luminosity for dust.

In equations (4) and (5) the drag force is approximately expressed as (Lamers, Cassinelli 1999)

$$f_{\text{drag}} = \rho n_d \sigma_d v_{\text{drift}} \sqrt{c_s^2 + v_{\text{drift}}^2}, \quad (7)$$

where $n_d (= \nu / m_d)$ is the number density of dust, v_{drift} the drift velocity between dust and gas:

$$v_{\text{drift}} = u - v, \quad (8)$$

and c_s the sound speed of gas: $c_s = \sqrt{\partial p / \partial \rho}$.

Inserting the drag force (7), equations (4) and (5) are explicitly expressed as

$$v \frac{dv}{dr} = -\frac{1}{\rho} \frac{dp}{dr} - \frac{GM}{r^2} + \frac{\sigma_d}{m_d} v(u-v) \sqrt{c_s^2 + (u-v)^2}, \quad (9)$$

$$u \frac{du}{dr} = -\frac{GM(1-\Gamma)}{r^2} - \frac{\sigma_d}{m_d} \rho(u-v) \sqrt{c_s^2 + (u-v)^2}. \quad (10)$$

2.4. Energy Equation

The energy equation for the gas component is expressed as

$$\frac{1}{r^2} \frac{d}{dr} \left(r^2 \frac{p}{\gamma - 1} v \right) + p \frac{1}{r^2} \frac{d}{dr} (r^2 v) = q, \quad (11)$$

where γ is the ratio of the specific heats, q the heating rate, generally including the energy exchange with the radiation field, frictional heating, exothermic chemical reactions on the surface of dust grains, and so on. For the present purpose, we only consider the frictional heating q_{fric} between dust and gas (Krüger et al. 1994). Hence, the heating rate is approximately written as

$$q = q_{\text{fric}} = v_{\text{drift}} f_{\text{drag}}. \quad (12)$$

The dust temperature T_d is roughly determined by the radiative equilibrium between dust and radiation fields,

$$T_d^4 = T_{\text{rad}}^4 = \frac{1}{2} T_*^4 \left(1 - \sqrt{1 - \frac{R_*^2}{r^2}} \right), \quad (13)$$

where T_* and R_* is the temperature and size of the central radiating region.

Finally, equation of state to close the equation set is

$$p = \frac{\mathcal{R}}{\mu} \rho T, \quad (14)$$

where \mathcal{R} is the gas constant, μ the mean molecular weight, and T the gas temperature.

2.5. Wind Equation

According to the usual procedure for transonic flow, we first derive the *wind equation*, an ordinary differential equation of the first order on the variable. From the equation of motion (9)

and the energy equation (11), we can derive a set of wind equations on v and c_s . After some manipulations, we have wind equations for the present case:

$$(v^2 - c_s^2) \frac{dv}{dr} = v \left[\frac{2}{r} c_s^2 - \frac{GM}{r^2} + \frac{\sigma_d}{m_d} v(u - v) \sqrt{c_s^2 + (u - v)^2} - \frac{\gamma - 1}{\rho v} q \right], \quad (15)$$

$$(v^2 - c_s^2) \frac{dc_s^2}{dr} = (\gamma - 1) c_s^2 \left[-\frac{2}{r} v^2 + \frac{GM}{r^2} - \frac{\sigma_d}{m_d} v(u - v) \sqrt{c_s^2 + (u - v)^2} + \frac{\gamma v^2 / c_s^2 - 1}{\rho v} q \right]. \quad (16)$$

Here, we have used the relation on the sound speed: $c_s^2 = \gamma p / \rho = \gamma (\mathcal{R} / \mu) T$.

In equations (15) and (16), the second lines on the right-hand sides are terms originating from the drag force, and the third lines are those of momentum change due to frictional heating. In the case of accreting flow ($u, v < 0$), the critical points shift outwards due to the drag force when the dust velocity is greater than the gas velocity ($|u| > |v|$), and vice versa. On the other hand, the critical points shift inwards due to frictional heating.

Within the parameter ranges considered in this paper, however, the variation in the radius of transonic points is not very large. That is, the transonic point r_c is almost located at the Bondi radius,

$$r_c \sim \frac{GM}{2c_{sc}^2} = \frac{5 - 3\gamma}{4} \frac{GM}{c_{s\infty}^2}, \quad (17)$$

and the sound speed there is almost equal to the Bondi case,

$$c_{sc}^2 \sim \frac{2}{5 - 3\gamma} c_{s\infty}^2, \quad (18)$$

where $c_{s\infty}$ is the sound speed at infinity.

2.6. Method of Solution

Consequently, the basic equations of the present dust–gas accretion onto a luminous central object are equations (2), (3), (15), (16), (10), and (14) on variables ρ, v, u, c_s, u , and p . The parameters are apparently $\gamma, \mu, \dot{M}, \dot{M}_d$, and Γ ; the accretion rate is determined as an eigenvalue of the differential equation.

In order to solve these basic equations, we should impose boundary conditions. For accreting flow from an infinite distance to the center, the temperature and sound speed become asymptotically constant at large distance from the center: $c_s \rightarrow c_{s\infty}$ and $T \rightarrow T_\infty$ at $r \rightarrow \infty$. Similarly, $\rho \rightarrow \rho_\infty$ at $r \rightarrow \infty$ (i.e., the number density $n \rightarrow n_\infty$ at $r \rightarrow \infty$). The gas velocity v is then given by continuity equation (2):

$$v \rightarrow v_\infty = -\frac{\dot{M}}{4\pi r^2 \rho_\infty} \quad (19)$$

at $r \rightarrow \infty$. The dust density is also constant at large distance: $v \rightarrow v_\infty$ at $r \rightarrow \infty$. For the dust velocity u , on the other

hand, the gravitational force (modified by the radiation pressure) should be balanced by the drag force at large distance where the velocity is sufficiently small. Hence, from equation (10), we have the asymptotic form:

$$u \rightarrow u_\infty = \left[1 + \frac{4\pi GM}{(\sigma_d / m_d) \dot{M} c_{s\infty}} (1 - \Gamma) \right] v_\infty \quad (20)$$

at $r \rightarrow \infty$. Thus, we must arbitrarily give $c_{s\infty}, \rho_\infty$, and v_∞ , as additional parameters.

Starting from these boundary conditions, we can solve the basic equations inwards by the shooting method. Namely, with a trial value of the accretion rate \dot{M} , the basic equations are integrated inwards. For a wrong value of \dot{M} , the integrated solution misses the critical point. Then, the trial value is changed. When the value of \dot{M} is sufficiently close to the correct value, the solution approaches the critical point. In the present case of a system of differential equations, a transonic point is generally a saddle type with a first-order singularity and a nodal type with a higher order singularity does not appear (cf. Kato et al. 1998). We thus get over the critical point under a linear approximation. Beyond the critical points, the integration of wind equations is resumed. During the above-mentioned procedures, the gas accretion rate \dot{M} is determined as an eigenvalue.

2.7. Normalization

In order to apply the present flow to several distinct systems of accretion, let us normalize the basic equations as follows. Since we consider the accretion flow ($u, v < 0$), let us take the absolute value of velocities: $u \rightarrow |u|$ and $v \rightarrow |v|$. The length, velocity, and density are respectively measured in units of $R, \sqrt{GM/R}$, and ρ_∞ , where R is some reference radius and ρ_∞ the gas density at infinity.

Then, the basic equations [(2), (3), (15), (16), and (10)] are rewritten as

$$r^2 \rho v = \dot{\mathcal{M}}, \quad (21)$$

$$r^2 v u = \dot{\mathcal{M}}_d, \quad (22)$$

$$(v^2 - c_s^2) \frac{dv}{dr} = v \left[\frac{2}{r} c_s^2 - \frac{1}{r^2} - \frac{\Delta_d}{r^2} \frac{u - v}{u} w + (\gamma - 1) \frac{\Delta_d}{r^2} \frac{(u - v)^2}{uv} w \right], \quad (23)$$

$$(v^2 - c_s^2) \frac{dc_s^2}{dr} = (\gamma - 1) c_s^2 \left[-\frac{2}{r} v^2 + \frac{1}{r^2} + \frac{\Delta_d}{r^2} \frac{u - v}{u} w - \left(\gamma \frac{v^2}{c_s^2} - 1 \right) \frac{\Delta_d}{r^2} \frac{(u - v)^2}{uv} w \right]. \quad (24)$$

$$u \frac{du}{dr} = -\frac{1 - \Gamma}{r^2} + \frac{\Delta}{r^2} \frac{u - v}{v} w, \quad (25)$$

where

$$\dot{\mathcal{M}} = \frac{\dot{M}}{4\pi R^2 \rho_\infty \sqrt{GM/R}}, \quad (26)$$

$$\dot{\mathcal{M}}_d = \frac{\dot{M}_d}{4\pi R^2 \rho_\infty \sqrt{GM/R}}, \quad (27)$$

Table 1. Typical parameters.

	Protostar	Black hole	AGN/Sy
M	$1 M_\odot$	$10 M_\odot$	$10^5 M_\odot$
R	$1 R_\odot$	$10^{10} r_g$	$10^{10} r_g$
$\sqrt{GM/R}$	437 km s^{-1}	2.12 km s^{-1}	2.12 km s^{-1}
L	$\sim 10 L_\odot$	$\lesssim L_E$	$\lesssim L_E$
Γ	~ 0.78	$\lesssim 10^3$	$\lesssim 10^3$
T_∞	100 K	100 K	100 K
$c_{s\infty}$	0.763 km s^{-1}	0.763 km s^{-1}	0.763 km s^{-1}
n_∞	10 cm^{-3}	10 cm^{-3}	10 cm^{-3}
v_∞/ρ_∞	0.01	0.01	0.01

Note. r_g : Schwarzschild radius of the central object. L_E : Eddington luminosity for normal plasmas.

$$\Delta = \frac{(\sigma_d/m_d)\dot{M}}{4\pi\sqrt{GMR}}, \quad (28)$$

$$\Delta_d = \frac{(\sigma_d/m_d)\dot{M}_d}{4\pi\sqrt{GMR}}, \quad (29)$$

$$w = \sqrt{c_s^2 + (u - v)^2}, \quad (30)$$

and the symbols for the absolute values, say “ $|v|$ ”, or for the dimensionless variables, say “ \hat{v} ”, are dropped for simplicity.

The asymptotic solution (20) is expressed as

$$u_\infty = \left(1 + \frac{1 - \Gamma}{\Delta c_{s\infty}}\right) v_\infty \quad (31)$$

in dimensionless variables. This asymptotic solution yields the condition for accretion rates and nondimensional parameters,

$$\frac{\dot{M}_d}{\dot{M}} = \frac{\dot{M}_d}{\dot{M}} = \frac{\Delta_d}{\Delta} = \frac{v_\infty}{\rho_\infty} \left(1 + \frac{1 - \Gamma}{\Delta c_{s\infty}}\right). \quad (32)$$

Hence, for fixed M and R , we must set the parameters γ , μ , L (or Γ), and the boundary values $c_{s\infty}$ (or T_∞), ρ_∞ (or n_∞), v_∞ (or v_∞/ρ_∞).

3. Results

We now examine dust–gas accretion onto the luminous central object. As already stated and shown below, in the present regime of parameters the gas flow is almost Bondi type and the flow pattern can be scaled in terms of the critical radius, although the dust flow is not. For convenience, we separately discuss the two main cases: the protostar and black-hole accretions.

In table 1, we first summarize the values of the parameters adopted in this paper for several related astronomical systems. Throughout this paper, we set $\gamma = 7/5$, $\mu = 2$ (hydrogen molecule), $\sigma_d/m_d = 10^5$, and $\kappa_d = 10^3$ ($Q_A = 0.01$). The temperature T_∞ , the gas number density n_∞ , and the dust-to-gas ratio v_∞/ρ_∞ at infinity in table 1 are typical values.

3.1. Protostar Accretion

In figure 1, a typical example is shown for the case of (non-luminous) protostar accretion: the mass $M = 1 M_\odot$ and the

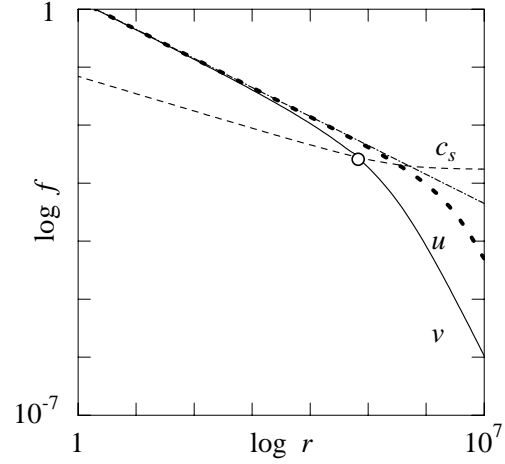


Fig. 1. Typical example for protostar accretion: the central mass and reference radius are $M = 1 M_\odot$ and $R = 1 R_\odot$. A thin solid curve represents the gas infall velocity v , a thin dashed one denotes the sound speed c_s , and a thick dotted one means the dust infall velocity u . A chain-dotted line is the freefall velocity. An open circle marks a transonic point. The other parameters are $T_\infty = 100 \text{ K}$, $n_\infty = 10 \text{ cm}^{-3}$, $v_\infty/\rho_\infty = 0.01$, and $\Gamma = 0$.

reference radius $R = 1 R_\odot$. A thin solid curve represents the gas infall velocity v , a thin dashed one denotes the sound speed c_s , and a thick dotted one means the dust infall velocity u in units of $\sqrt{GM/R}$. A chain-dotted line is the freefall velocity. The parameters are $T_\infty = 100 \text{ K}$, $n_\infty = 10 \text{ cm}^{-3}$, $v_\infty/\rho_\infty = 0.01$, and $\Gamma = 0$. In this case the gas and dust accretion rates are determined as $\dot{M} = 0.747 \times 10^{-10} M_\odot \text{ yr}^{-1}$ and $\dot{M}_d = 0.355 \times 10^{-10} M_\odot \text{ yr}^{-1}$, respectively.

As already stated, the gas inflow is almost (adiabatic) Bondi-like accretion. Outside the transonic point the gas flow is almost hydrostatic and uniform density and the infall velocity varies as $v \propto r^{-2}$, whereas the gas infall velocity approaches freefall inside the transonic point. On the other hand, the dust is pressureless. Due to the drag force exerted by the gas, however, the dust infall velocity becomes smaller than the freefall velocity in the outer region, although it also varies as $u \propto r^{-2}$. The dust infall velocity approaches the freefall value in the inner region.

In this example of figure 1, the dust-to-gas ratio is small ($v_\infty/\rho_\infty = 0.01$), but the magnitude of the dust infall velocity u is large. As a result, the dust accretion rate is comparable to the gas accretion rate.

The parameter dependence is shown in figure 2. Figure 2a shows the dependence on the gas density $\rho_\infty (= mn_\infty)$ at infinity. The values of the gas number density n_∞ are attached to each curve. The other parameters are typical values ($T_\infty = 100 \text{ K}$, $v_\infty/\rho_\infty = 0.01$, $\Gamma = 0$). As n_∞ increases, the drag force becomes large and the dust infall velocity approaches the gas infall velocity, although the gas infall velocity does not change very much. Figure 2b shows the dependence on the gas temperature T_∞ at infinity. The values of T_∞ are attached to each curve. The other parameters are typical values ($n_\infty = 10 \text{ cm}^{-3}$, $v_\infty/\rho_\infty = 0.01$, $\Gamma = 0$). As T_∞ increases, the transonic radius becomes small and the outer quasi-hydrostatic region extends inwards, like the usual Bondi accretion. The dust accre-

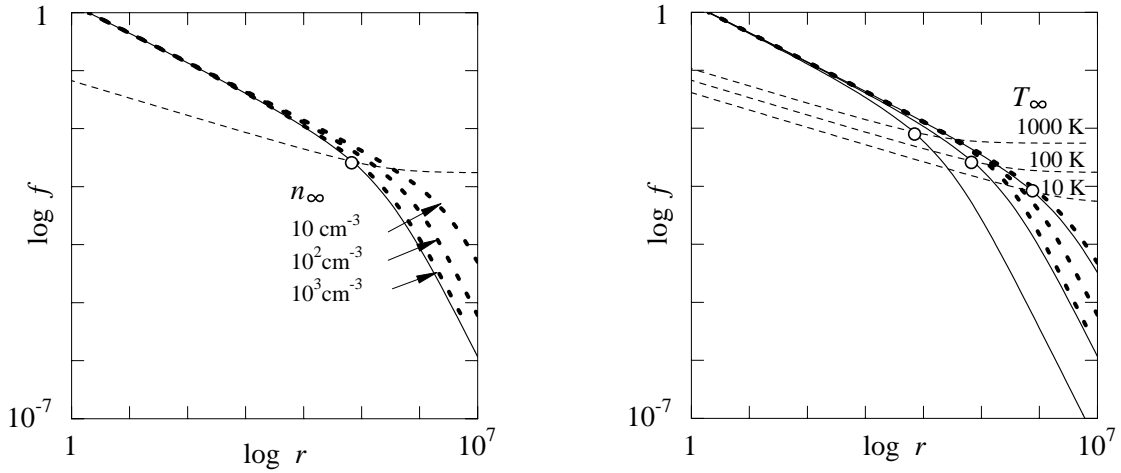


Fig. 2. Parameter dependence of the dynamical properties on (a) n_∞ and (b) T_∞ . The other parameters are typical values.

Table 2. Accretion rates for protostar accretion ($\Gamma = 0$).

n_∞	v_∞/ρ_∞	\dot{M}	\dot{M}_d	$\dot{M} + \dot{M}_d$
$T_\infty = 10 \text{ K}$				
10	0	25.5	0.	25.5
	0.001	25.0	0.14	25.1
	0.01	24.5	1.34	25.8
100	0	230.0	0	230.0
	0.001	229.0	0.34	229.3
	0.01	230.5	3.40	233.9
1000	0	2300	0	2300
	0.001	2290	2.40	2292
	0.01	2310	24.20	2334
$T_\infty = 100 \text{ K}$				
10	0	0.833	0	0.83
	0.001	0.813	0.036	0.85
	0.01	0.747	0.355	1.10
100	0	8.66	0	8.66
	0.001	8.24	0.043	8.28
	0.01	8.20	0.429	8.63
1000	0	80.9	0	80.9
	0.001	80.9	0.116	81.0
	0.01	82.5	1.172	83.7
$T_\infty = 1000 \text{ K}$				
10	0	0.0265	0	0.027
	0.001	0.0255	0.011	0.036
	0.01	0.0193	0.110	0.129
100	0	0.265	0	0.265
	0.001	0.257	0.011	0.268
	0.01	0.237	0.112	0.349
1000	0	2.650	0	2.650
	0.001	2.577	0.014	2.591
	0.01	2.550	0.135	2.685

Note. The number density n_∞ is in units of cm^{-3} . The accretion rates are in units of $10^{-10} M_\odot \text{ yr}^{-1}$.

Table 3. Accretion rates for protostar accretion ($\Gamma \geq 0$).

Γ	\dot{M}	\dot{M}_d	$\dot{M} + \dot{M}_d$
0.0	0.747	0.355	1.102
0.1	0.758	0.320	1.078
0.2	0.770	0.286	1.056
0.3	0.782	0.251	1.033
0.4	0.794	0.216	1.010
0.5	0.802	0.182	0.984
0.6	0.815	0.147	0.962
0.7	0.816	0.112	0.928
0.8	0.816	0.078	0.894
0.9	0.819	0.043	0.862
1.0	0.820	0.008	0.828
1.01	0.826	0.005	0.831
1.02	0.827	0.001	0.828

Note. The case of $T_\infty = 100 \text{ K}$, $n_\infty = 10 \text{ cm}^{-3}$, and $v_\infty/\rho_\infty = 0.01$. The accretion rates are in units of $10^{-10} M_\odot \text{ yr}^{-1}$.

tion is also somewhat affected by the change of T_∞ . Finally, the dust-to-gas ratio v_∞/ρ_∞ has a slight influence on the dynamical properties, although the accretion rates are changed as shown below.

The accretion rates obtained for a non-luminous case are summarized in table 2. As T_∞ increases, the subsonic regime extends and the gas infall velocity decreases, and therefore the gas accretion rate \dot{M} reduces. It is roughly proportional to n_∞ , as expected from the continuity equation. The increase in v_∞/ρ_∞ leads a slight decrease in \dot{M} . This can be understood as follows. In the wind equation (23) the gas flow is slightly accelerated by the drag term and decelerated by the frictional heating term, and the latter slightly overcomes the former. As a result, the gas flow is slightly decelerated due to the existence of the gas-dust interaction and the gas accretion rate is reduced with v_∞/ρ_∞ .

As for the dust accretion rate \dot{M}_d , it is greatly influenced by the gas temperature at infinity, T_∞ . That is, as T_∞ increases,

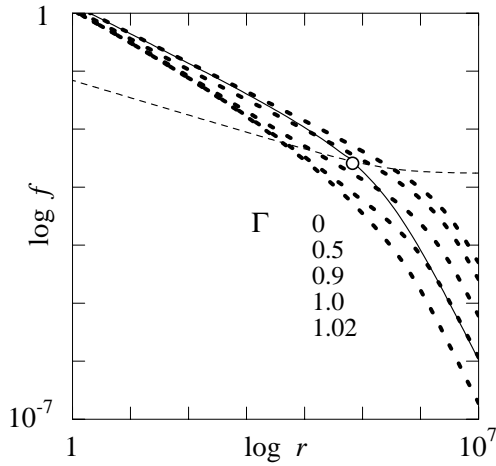


Fig. 3. Luminosity dependence of the flow: the dust–gas accretion onto a luminous source. Thick dotted curves denote the dust infall velocities: from top to bottom $\Gamma = 0, 0.5, 0.9, 1.0$, and 1.02 . The other parameters are $T_\infty = 100$ K, $n_\infty = 10$ cm $^{-3}$, and $v_\infty/\rho_\infty = 0.01$.

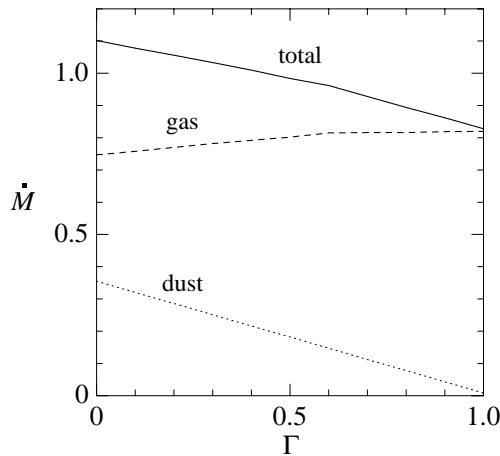


Fig. 4. Accretion rates for protostar accretion. The abscissa is the normalized luminosity Γ , whereas the ordinate is the gas, dust, and total accretion rates in units of $10^{-10} M_\odot$ yr $^{-1}$. The other parameters are $T_\infty = 100$ K, $n_\infty = 10$ cm $^{-3}$, and $v_\infty/\rho_\infty = 0.01$.

the dust accretion rate decreases, associating to the decrease in the gas accretion rate. The dust accretion rate does not depend very much on the change in the gas number density at infinity, n_∞ . Finally, it is nearly proportional to the dust-to-gas ratio, v_∞/ρ_∞ , as is easily seen.

Figure 3 shows the luminosity dependence: the dust–gas accretion onto a luminous source. In figure 3 thick dotted curves show the dust infall velocities for several normalized luminosity Γ (from top to bottom 0, 0.5, 0.9, 1.0, and 1.02). The dust accretion is considerably affected by the central luminosity. As Γ increases, the dust infall velocity is suppressed due to radiation pressure.

The effect of radiation is also reflected in the accretion rates. The accretion rates obtained for luminous cases are summarized in table 3 and shown in figure 4. As Γ increases, the gas accretion rate slightly increases, but the dust accretion rate

Table 4. Accretion rates for black-hole accretion ($\Gamma = 0$).

	n_∞	v_∞/ρ_∞	\dot{M}	\dot{M}_d	$\dot{M} + \dot{M}_d$
$T_\infty = 100$ K					
10	0		81.0	0	81.0
	0.001		81.0	0.428	81.4
	0.01		79.5	4.268	83.8
100	0		810.0	0	810.0
	0.001		810.0	1.157	811.2
	0.01		815.0	11.623	826.6
1000	0		7780	0	7780
	0.001		7700	8.047	7708
	0.01		7800	81.47	7881

Note. The number density n_∞ is in units of cm $^{-3}$. The accretion rates are in units of $10^{-10} M_\odot$ yr $^{-1}$.

Table 5. Accretion rates for black-hole accretion ($\Gamma \geq 0$).

Γ	\dot{M}	\dot{M}_d	$\dot{M} + \dot{M}_d$
0.0	79.5	4.268	83.8
0.1	80.2	3.928	84.1
0.2	80.9	3.588	84.5
0.3	81.0	3.241	84.2
0.4	81.2	2.896	84.1
0.5	81.2	2.549	83.7
0.6	81.3	2.202	83.5
0.7	81.4	1.856	83.3
0.8	81.4	1.509	82.9
0.9	81.5	1.162	82.7
1.0	81.6	0.816	82.4
1.1	81.6	0.469	82.1
1.2	81.7	0.122	81.8

Note. The case of $T_\infty = 100$ K, $n_\infty = 10$ cm $^{-3}$, and $v_\infty/\rho_\infty = 0.01$. The accretion rates are in units of $10^{-10} M_\odot$ yr $^{-1}$.

decreases. As a result, the total accretion rate decreases. In particular, the dust accretion rate is roughly proportional to $(1 - \Gamma)$, as shown in figure 4. This point is discussed in a later section. Another point is the possible *super-Eddington* accretion for a very limited range ($\Gamma \lesssim 1.02$). Generally speaking, the dust particles cannot accrete when the central luminosity exceeds the Eddington one for dust. In the present case, where the drag force operates, the dust flow can accrete even if the luminosity slightly exceeds the Eddington one.

3.2. Black-Hole Accretion

In figure 5, typical examples are shown for the case of black-hole accretion: the mass $M = 10 M_\odot$ and the reference radius $R = 10^{10} r_g \sim 0.01$ pc. A thin solid curve represents the gas infall velocity v , a thin dashed one denotes the sound speed c_s , and thick dotted ones mean the dust infall velocity u in units of $\sqrt{GM/R}$. The values of the normalized luminosity Γ for thick dotted curves are 0, 0.5, 0.9, 1.0, and 1.2 from top to bottom. The other parameters are $T_\infty = 100$ K, $n_\infty = 10$ cm $^{-3}$, and $v_\infty/\rho_\infty = 0.01$. In this case the gas and dust accretion rates are determined to be $\dot{M} = 79.5 \times 10^{-10} M_\odot$ yr $^{-1}$ and $\dot{M} =$

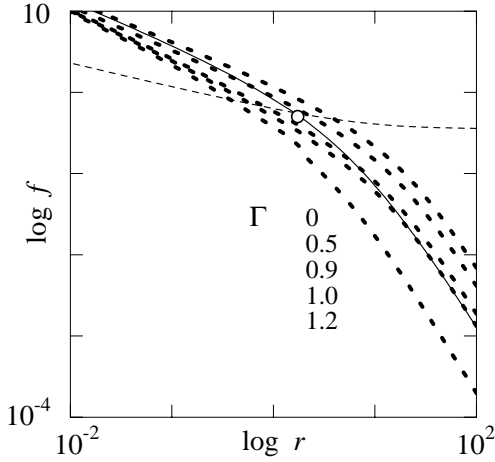


Fig. 5. Typical example for black-hole accretion: the central mass and reference radius are $M = 10 M_{\odot}$ and $R = 10^{10} r_g$. A thin solid curve represents the gas infall velocity v , a thin dashed one denotes the sound speed c_s , and thick dotted ones mean the dust infall velocity u (from top to bottom $\Gamma = 0, 0.5, 0.9, 1.0$, and 1.2). The other parameters are $T_{\infty} = 100$ K, $n_{\infty} = 10 \text{ cm}^{-3}$, and $v_{\infty}/\rho_{\infty} = 0.01$.

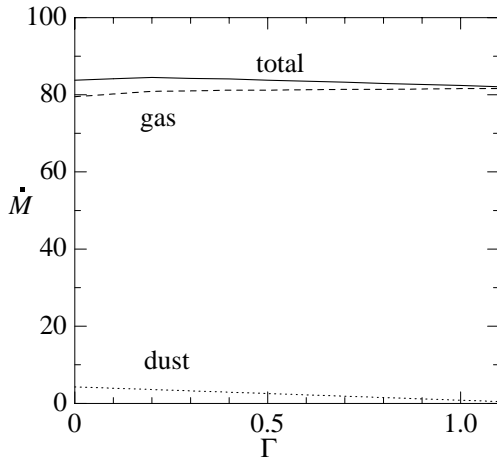


Fig. 6. Accretion rates for black-hole accretion. The abscissa is the normalized luminosity Γ , whereas the ordinate is the gas, dust, and total accretion rates in units of $10^{-10} M_{\odot} \text{ yr}^{-1}$. The other parameters are $T_{\infty} = 100$ K, $n_{\infty} = 10 \text{ cm}^{-3}$, and $v_{\infty}/\rho_{\infty} = 0.01$.

$4.27 \times 10^{-10} M_{\odot} \text{ yr}^{-1}$, respectively, for the case of $\Gamma = 0$.

The accretion nature is similar to the case of protostar accretion, although the quantitative values, such as accretion rates, are quite different.

The accretion rates obtained for the non-luminous case are summarized in table 4. Compared with table 2, both the gas and dust accretion rates in table 4 increase, although the increasing ratios are different. That is, the gas accretion rate for black-hole accretion becomes about 100-times larger than that for protostar accretion, while the dust accretion rate is about 10-times larger. This is roughly explained as follows. The essential difference between the protostar case in table 2 and the black-hole case in table 4 is the mass of the central object: i.e., for the black hole case the mass of the central object is set to

Table 6. Results for typical parameters.

	Protostar	Black hole
M	$1 M_{\odot}$	$10 M_{\odot}$
R	$1 R_{\odot}$	$10^{10} r_g$
$\sqrt{GM/R}$	437 km s^{-1}	2.12 km s^{-1}
\dot{M}	$0.747 \times 10^{-10} M_{\odot} \text{ yr}^{-1}$	$79.5 \times 10^{-10} M_{\odot} \text{ yr}^{-1}$
\dot{M}_d	$0.355 \times 10^{-10} M_{\odot} \text{ yr}^{-1}$	$4.27 \times 10^{-10} M_{\odot} \text{ yr}^{-1}$
Δ	12.3	0.636
Δ_d	5.85	0.0341
\dot{M}_d/\dot{M}	0.475	0.0537
$\kappa_d \rho_{\infty} R$	1.16×10^{-8}	4.93×10^{-3}
$\kappa_d v_{\infty} R$	1.16×10^{-10}	4.93×10^{-5}

Note. The case of $T_{\infty} = 100$ K, $n_{\infty} = 10 \text{ cm}^{-3}$, and $v_{\infty}/\rho_{\infty} = 0.01$, $\Gamma = 0$.

be ten-times larger than that for the protostar case. The critical radius (17) is then linearly scaled up by a factor of 10. Since the accretion area is scaled up by a factor of the square of the length, the gas accretion rate increases by a factor of 100: it is roughly proportional to M^2 . On the other hand, the dust accretion is controlled by the drag force between the dust and gas. The dust infall velocity at infinity is determined by equation (20), and for the present parameter ranges the second term in equation (20) dominates: $u_{\infty} \propto (M/\dot{M})v_{\infty}$. Furthermore, since $v_{\infty} \propto \dot{M}$, u_{∞} is roughly proportional to M , and the dust accretion rate is also proportional to M .

The luminosity dependence is also examined. The accretion rates obtained for luminous cases are summarized in table 5 and shown in figure 6. Compared with the protostar case, the gas accretion rate becomes larger by a factor of ~ 100 , whereas the dust accretion rate increases by a factor of ~ 10 . Hence, the fraction of dust in the total accretion rate becomes small.

4. Discussion

As a first step towards a discussion, we summarize the results obtained for typical values in table 6. For the typical values adopted in the present paper, the nondimensional parameter Δ_d is less than Δ , and the drag interaction between the dust and gas is more important in dust than in gas. The dust accretion rate \dot{M}_d is smaller than the gas accretion rate \dot{M} for both the protostar and black-hole cases. Furthermore, the ratio of the dust accretion rate to the gas accretion rate, \dot{M}_d/\dot{M} , becomes smaller as M increases. This is because the gas accretion rate is roughly proportional to M^2 , while the dust accretion rate is proportional to M , as already noted. Hence, their ratio is proportional to M^{-1} .

As for the luminosity dependence, the gas accretion rate is insensitive to the central luminosity, while the dust accretion rate linearly decreases with an increase in Γ .

Taking account of all these factors as well as the numerical results discussed in the previous section, we can heuristically write down the approximate expressions for the accretion rates:

$$\dot{M} \sim 0.8 \times 10^{-10} M_{\odot} \text{ yr}^{-1} \left(\frac{M}{1 M_{\odot}} \right)^2 \times \left(\frac{T_{\infty}}{100 \text{ K}} \right)^{-3/2} \left(\frac{n_{\infty}}{10 \text{ cm}^{-3}} \right)^1, \quad (33)$$

$$\dot{M}_d \sim 0.4 \times 10^{-10} M_\odot \text{ yr}^{-1} \left(\frac{M}{1 M_\odot} \right)^1 \times \left(\frac{T_\infty}{100 \text{ K}} \right)^{-1/2} \left(\frac{v_\infty/\rho_\infty}{0.01} \right)^1 (1 - \Gamma). \quad (34)$$

The ratio is then

$$\frac{\dot{M}_d}{\dot{M}} \sim 0.5 \left(\frac{M}{1 M_\odot} \right)^{-1} \left(\frac{T_\infty}{100 \text{ K}} \right)^1 \times \left(\frac{n_\infty}{10 \text{ cm}^{-3}} \right)^{-1} \left(\frac{v_\infty/\rho_\infty}{0.01} \right)^1 (1 - \Gamma). \quad (35)$$

As long as the normalized luminosity Γ for dust is less than unity, these expressions may be applicable to wide ranges of parameters.

We discuss several other points. In this paper we assume that, at least for dust, the flow is optically thin. The flow is roughly divided into the outer quasi-hydrostatic region of $r_c \lesssim r \lesssim r_{\text{out}}$, where the density is almost uniform, and the inner freefall region of $r_{\text{in}} \lesssim r \lesssim r_c$, where the infall velocity is approximately a freefall one. The optical depth τ_d for dust is roughly evaluated as follows:

$$\begin{aligned} \tau_d &= \int_{r_{\text{in}}}^{r_{\text{out}}} \kappa_d v dr \\ &\sim \int_{r_{\text{in}}}^{r_c} \frac{\kappa_d \dot{M}_d}{4\pi r^2 u} dr + \int_{r_c}^{r_{\text{out}}} \kappa_d v_\infty dr \\ &\sim \frac{\kappa_d \dot{M}_d}{4\pi \sqrt{GM(1-\Gamma)}} \left(\frac{2}{\sqrt{r_{\text{in}}}} - \frac{2}{\sqrt{r_c}} \right) + \kappa_d v_\infty (r_{\text{out}} - r_c) \\ &\lesssim \frac{\Delta_d Q_A}{\sqrt{1-\Gamma}} \frac{2}{\sqrt{r_{\text{in}}/R}} + \kappa_d v_\infty R \frac{r_{\text{out}}}{R}. \end{aligned} \quad (36)$$

Using the results for typical parameters in table 6, the values of $\kappa_d v_\infty R$ are very small for both the protostar and black-hole cases and, therefore, the optical depth in the outer region is sufficiently small. In the inner region, on the other hand, the optical depth becomes large. For the case of protostar accretion, $\Delta_d Q_A \sim 0.058$ and the optical depth is less than unity for $r_{\text{in}}(1-\Gamma) \gtrsim 0.01 R = 0.01 R_\odot$. Hence, the assumption is valid in almost the relevant region. For the case of black-hole accretion, $\Delta_d Q_A \sim 0.00034$ and the optical depth is less than unity for $r_{\text{in}}(1-\Gamma) \gtrsim 10^{-7} R = 10^3 r_g$. Hence, the central region becomes optically thick, although the size is sufficiently smaller than the critical radius and the present results, such as accretion rates, are not changed.

We finally discuss the central luminosity L (or Γ). If the central object is a protostar or a neutron star and it shines, itself, the central luminosity is given as an independent parameter. If, however, the central luminosity is produced via the accretion energy, then the luminosity should be related to the accretion rate by $L = \eta \dot{M}_{\text{tot}} c^2 = \eta (\dot{M} + \dot{M}_d) c^2$, where η is the efficiency of the release of gravitational energy.

In the present problem for a prior given luminosity (as well as other parameters), the accretion rate is determined as an eigenvalue. The accretion luminosity obtained by this resultant accretion rate is not generally consistent with the luminosity given as a parameter. For example, for a non-relativistic object, such as protostars, the efficiency is $\eta = GM/r_* c^2$ (or $L = GM \dot{M}_{\text{tot}}/r_*$), where r_* is the radius of the central star, and

the normalized luminosity determined by equation (6) should become

$$\Gamma = 2.40 \times 10^{-4} \frac{\kappa_d}{10^3} \left(\frac{r_*}{R} \right)^{-1} \frac{\dot{M}_{\text{tot}}}{10^{-10} M_\odot \text{ yr}^{-1}}. \quad (37)$$

This is rather small and for a non-relativistic object the accretion luminosity may be negligible in such a present problem. For a relativistic object, such as black holes, on the other hand,

$$\Gamma = 0.646 \frac{\eta}{0.057} \frac{\kappa_d}{10^3} \left(\frac{M}{10 M_\odot} \right)^{-1} \frac{\dot{M}_{\text{tot}}}{10^{-10} M_\odot \text{ yr}^{-1}}. \quad (38)$$

This may become rather large.

When the accretion luminosity exceeds the assumed luminosity, there may occur several possible situations. One possibility is a breakdown of the stationarity. In the outer region, almost quasi-stationary accretion of dust and gas is established under the initial circumstances. Once the accreting gas reaches the central region, the accreting luminosity increases, and the dynamical structure of (dust) flow in the outer region may be drastically changed. Another possibility is a selective influence on dust grains. In the present analysis we first assumed that the dust size is uniform ($a_d = 0.05 \mu\text{m}$). In general, however, the dust size distributes in some ranges. As the dust size becomes large, the dust opacity κ_d becomes small and the normalized luminosity Γ also becomes small. Hence, for some accretion luminosity, the dust grains with small size cannot accrete, while the large grains can selectively accrete to adjust to a new stationary state.

5. Concluding Remarks

In this paper we have examined the spherical accretion of dust and gas onto a central gravitating object, taking into account the influence of a central luminosity. We summarize the main results:

1. The effect of dust on the gas flow is small and the gas flow is almost adiabatic Bondi type, as long as the central luminosity is less than the Eddington luminosity for dust.
2. The dust flow, on the other hand, is considerably affected by the gas flow. As the dust-to-gas ratio increases, the gas accretion rate slightly decreases and the dust accretion rate increases; the total accretion rate increases.
3. The dust flow is also remarkably affected by central radiation. As the luminosity increase, due to the existence of radiation pressure, the dust accretion rate linearly decreases; the total accretion rate then decreases with luminosity.
4. Accretion rates are approximately expressed by use of fundamental parameters: M , T_∞ , n_∞ , v_∞/ρ_∞ , and Γ .

In the present analysis, for simplicity, we have assumed that the dust size is uniform. In interstellar dust the size distribution, derived from the interstellar extinction curve, is $n(a_d) da_d \propto a_d^{-3.5} da_d$ (Evans 1993). In circumstellar dust the grain size may be a function of the distance from the central star. Recently, in order to examine the role of dust in the early epochs of the universe, Todini and Ferrara (2000) calculated the formation of dust in type II supernovae with primordial abundances. They found that the dust grains are made

of silicates (Mg_2SiO_4), amorphous carbon grains (ACG), magnetite (Fe_3O_4), and corundum (Al_2O_3). The sizes of these solid compounds distribute around $0.03\ \mu\text{m}$ for ACG and around $0.001\text{--}0.002\ \mu\text{m}$. As stated, the dust opacity and radiative effect strongly depend on the grain size.

In the present study, the temperature, density, and dust ratio at infinity are set to be typical interstellar values. In warmer circumstances dust evaporation and destruction may take place outside the critical points. In denser circumstances the dust flow may become optically thick. For a high dust-to-gas ratio the topological nature of the critical points may change in quality.

Moreover, when the central luminosity exceeds the Eddington one for dust, the dynamical nature of the dust may change. In particular, if the central object is a luminous accretion disk surrounding a gravitating object, the situation would drastically change, as has been shown for classical Hoyle–Lyttleton accretion (Fukue, Ioroi 1999; Hanamoto et al. 2001). The whole space would be divided into an inflow region near to the equator and an outflow region near to the axis. These should be examined in the future.

The author would like to thank an anonymous referee for useful comments which improved the original manuscript.

References

- Berruyer, N., & Frisch, H. 1983, *A&A*, 126, 269
 Bondi, H. 1952, *MNRAS*, 112, 195
 Burger, H. L., & Katz, J. I. 1980, *ApJ*, 236, 921
 Evans, A. 1992, *The Dusty Universe* (New York: Ellis Horwood), ch. 6
 Flammang, R. A. 1982, *MNRAS*, 199, 833
 Fukue, J., & Ioroi, M. 1999, *PASJ*, 51, 151
 Fukue, J., & Umemura, M. 1995, *PASJ*, 47, 429
 Gail, H. P., & Sedlmayr, E. 1987, *A&A*, 171, 197
 Gilman, R. C. 1972, *ApJ*, 178, 423
 Goldreich, P., & Scoville, N. 1976, *ApJ*, 205, 144
 Hanamoto, K., Ioroi, M., & Fukue, J. 2001, *PASJ*, 53, 105
 Henriksen, R. N., & Heaton, K. C. 1975, *MNRAS*, 171, 27
 Kato, S., Fukue, J., & Mineshige, S. 1998, *Black-Hole Accretion Disks* (Kyoto: Kyoto University Press)
 Krüger, D., Gauger, A., & Sedlmayr, E. 1994, *A&A*, 290, 573
 Lamers, H. J. G. L. M., & Cassinelli, J. P. 1999, *Introduction to Stellar Winds* (Cambridge: Cambridge University Press), ch. 7
 MacGregor, K. B., & Stencel, R. E. 1992, *ApJ*, 397, 644
 Netzer, N., & Elitzur, M. 1993, *ApJ*, 410, 701
 Nio, T., Matsuda, T., & Fukue, J. 1998, *PASJ*, 50, 495
 Shakura, N. I., & Sunyaev, R. A. 1973, *A&A*, 24, 337
 Shapiro, S. L. 1973, *ApJ*, 180, 531
 Taam, R. E., Fu, A., & Fryxell, B. A. 1991, *ApJ*, 371, 696
 Tamazawa, S., Toyama, K., Kaneko, N., & Ono, Y. 1975, *Ap&SS*, 32, 403
 Tielens, A. G. G. 1983, *ApJ*, 271, 702
 Todini, P., & Ferrara, A. 2000, *MNRAS*, submitted
 Umemura, M., & Fukue, J. 1994, *PASJ*, 46, 567